Research Article | Vol. 27, No. 15 | 22 Jul 2019 | OPTICS EXPRESS 21083
Optics EXPRESS

Direct measurement of the spectral dependence of Lamb coupling constant in a dual frequency quantum well-based VECSEL

GAËLLE BRÉVALLE,[1] SALVATORE PES,[1] CYRIL PARANTHOËN,[1] MATHIEU PERRIN,[1] CHRISTOPHE LEVALLOIS,[1] CYRIL HAMEL,[1] ALEXANDRU MEREUTA,[2] ANDREI CALIMAN,[2] ELI KAPON,[2] ARTHUR VALLET,[3] LAURENT CHUSSEAU,[3] HERVÉ FOLLIOT,[1] AND MEHDI ALOUINI[1,*]

[1]*Univ Rennes, INSA Rennes, CNRS, Institut FOTON - UMR 6082, F-35000 Rennes, France*
[2]*Laboratory of Physics of Nanostructures, Ecole Polytechnique Fédérale de Lausanne, CH-1015 Lausanne, Switzerland*
[3]*IES, Université de Montpellier, CNRS, Montpellier, France*
** mehdi.alouini@univ-rennes1.fr*

Abstract: Spectral dependence of Lamb coupling constant *C* is experimentally investigated in an InGaAlAs Quantum Wells active medium. An Optically-Pumped Vertical-External-Cavity Surface-Emitting Laser is designed to sustain the oscillation of two orthogonally polarized modes sharing the same active region while separated in the rest of the cavity. This laser design enables to tune independently the two wavelengths and, at the same time, to apply differential losses in order to extract without any extrapolation the actual coupling constant. *C* is found to be almost constant and equal to 0.84 ± 0.02 for frequency differences between the two eigenmodes ranging from 45 GHz up to 1.35 THz.

1. Introduction

Lamb coupling constant *C* [1] introduced in 1964 is an important physical parameter in multimode lasers as it governs the dynamics of coupled modes. In particular, in dual-frequency lasers *C* rules the stability condition as well as the robustness of dual-frequency operation. These lasers are attractive sources for optical generation of high-purity Terahertz (THz) radiation [2], offering numerous applications including in radio-astronomy [3], environmental monitoring [4], communication [5], imaging and sensing in medicine, biology [6] and security [7]. In that respect, tunable dual-polarization solid-state lasers with active media such as Nd:YAG [8], Yb,Er:Glass [9] and Nd:YVO_4 [10] have been realized, alongside with the measurement of the Lamb coupling constant. For $C < 1$, simultaneous oscillation of two modes is possible. Nevertheless in practice, the dual-frequency oscillation becomes increasingly perturbed as *C* approaches 1 until reaching bistability when *C* exceeds 1 [11]. In solid-state lasers, *C* can be quite high, *C* ~0.8 in Er,Yb:glass [12,13] and ~0.85 in Nd:YVO_4 [10] or even quite weak: from 0.8 to 0.4 in Nd:YAG depending on the orientation of the crystallographic axes with respect to the laser polarizations [14].

In semiconductor active media, dual-polarization oscillation has been already demonstrated in semiconductor Quantum Well (QW) based Vertical External Cavity Surface Emitting Lasers (VECSELs), at 1 µm [15–17], at 852 nm [18,19], as well as at telecom wavelengths [20,21]. The use of such semiconductor structures in an external cavity enables class-A operation of the laser without relaxation oscillations leading naturally to low intensity noise oscillation. Owing to the anticipated high mode coupling, a spatial walk-off between the two modes is introduced in the active medium. To the best of our knowledge, the value of the coupling constant has been measured indirectly only once in a InGaAs/GaAsP QW based structure [22]. A coupling constant of 0.8 was found by extrapolating the effective coupling

#361824 https://doi.org/10.1364/OE.27.021083
Journal © 2019 Received 6 Mar 2019; revised 10 May 2019; accepted 27 May 2019; published 15 Jul 2019

Optics EXPRESS

constant obtained for different spatial separations. This value below 1 states that it is, in principle, possible to achieve the dual-frequency mode operation without any spatial walk-off, which is the first point that we want to experimentally address in this work. Moreover we wish to measure directly this coupling constant and to investigate its dependence with respect to the wavelength difference between the two modes.

We firstly describe the Optically-Pumped (OP) QW-based VECSEL and the experimental setup that has been conceived to perform the measurement of *C*. Secondly, we confirm that a dual-frequency operation can be obtained in QW-VECSELs without the need of spatial separation between the two modes in the active medium. Finally, we directly measure Lamb coupling constant for several wavelength differences, in a range as wide as 10.8 nm.

2. Experimental setup description and dual-frequency operation

The VECSEL structure comprises an InP-based gain region with 3 groups of 4-2-2 compressively strained InP/InAlGaAs QWs, which was wafer-fused to 19.5 pairs of AlAs/GaAs distributed Bragg reflector (DBR) [23]. Both InP-based active wafer and GaAs-based DBR wafer were grown separately by MOVPE. The VECSEL sub-cavity length was designed for emission around 1540-nm. The measured room temperature photoluminescence peak of the InAlGaAs QWs is centered near 1505-nm. After selective removal of the GaAs substrate, the DBR-side of the fused-structure was metalized with Ti/Au. The wafer was cleaved into ~3x3-mm chips and bonded to a metalized 5x5x0.3-mm diamond chip [24]. The InP substrate was then selectively etched. Finally, the gain mirror chip was mounted onto a copper heatsink.

The experimental setup in which the VECSEL structure is measured is depicted in Fig. 1. The gain mirror chip is mounted on a Peltier thermo-electric cooler, whose temperature is fixed to 20°C for all measurements. A 10 mm-thick YVO_4 birefringent crystal cut at 45° from its optical axis is inserted inside the cavity in order to introduce a d = 1 mm separation between the two orthogonally polarized eigenmodes of the cavity, except on the active medium where they overlap. The intensity of these two eigenmodes are noted I_1 (1-ordinary mode, linearly polarized along the x direction) and I_2 (2-extraordinary mode, linearly polarized along the y direction), as indicated in the figure. A single-mode pigtailed semiconductor diode laser, able to deliver up to 1 W at 975 nm, is used to continuously pump the active region of the chip. The linear polarization of the pump is oriented at 45° with respect to the x-axis in order to ensure that the two crossed polarization modes see a symmetrical pump contribution in terms of power and polarization. The pump is placed at an incident angle of 45° with respect to the VECSEL cavity axis and focused at the surface of the chip by two lenses. The cavity length is set at around 10 cm in order to ensure class-A operation of the laser. Due to the slight optical length difference between the two laser arms, the waist of the two orthogonal eigenmodes on the chip-side slightly differs from each other. They have been calculated to be ω_1 = 30 µm and ω_2 = 31 µm for a 113 mm-long cavity using the ray transfer matrix method for Gaussian modes propagation [25]. The pump beam is thus finely shaped to form an almost circular spot with semi-axis of 32 µm and 33 µm inside the active medium. These dimensions ensure that the two orthogonally-polarized eigenmodes have sufficient gain to simultaneously oscillate (see inset of Fig. 1). Furthermore, it promotes the two eigenmodes to oscillate on the fundamental transverse TEM_{00} profile.

At this point it is worth to notice that, unlike in [26] where each mode oscillates in a different cavity, it is here necessary to close the cavity with a planar output coupler on the side where the two eigenstates are spatially separated, to ensure that both modes are resonant after one cavity round-trip. The stability of the plane-plane resonator is then ensured by an intracavity fused silica bi-convex lens with a focal length of f = 20 mm, placed at 28 mm from the VECSEL chip. To force the single-frequency oscillation of the two eigenmodes, and thus reach a truly dual-frequency emission, a 100 µm-thick fused silica etalon with a reflectivity R_{eta} = 30% on both sides is inserted in each arm. Both etalons are mounted on a rotation stage

Optics EXPRESS

which, in addition, allows independent tuning of the emission wavelength of the corresponding eigenmode. A pinhole is also inserted between the active medium and the intra-cavity lens, i.e. where the two modes are spatially superimposed, in order to filter out any residual high-order transverse mode and ensure a perfect overlap of the two modes. To lower down as much as possible the optical losses, all the intra-cavity elements inserted in the laser resonator have been anti-reflection coated at the emission wavelength of the VECSEL. We also selected a planar output coupler with a relatively high reflectivity, of R = 99.5%. Two razor blades, mounted on two piezo-actuators allow introducing diffraction losses (a fraction of percent) on one arm without affecting the other (and vice versa). A low frequency sinusoidal voltage (f_{PZT} = 15-30 Hz) is applied to the piezo-actuators to slightly modulate the intensity of one eigenmode around its steady-state, as it will be further discussed in Section 3.

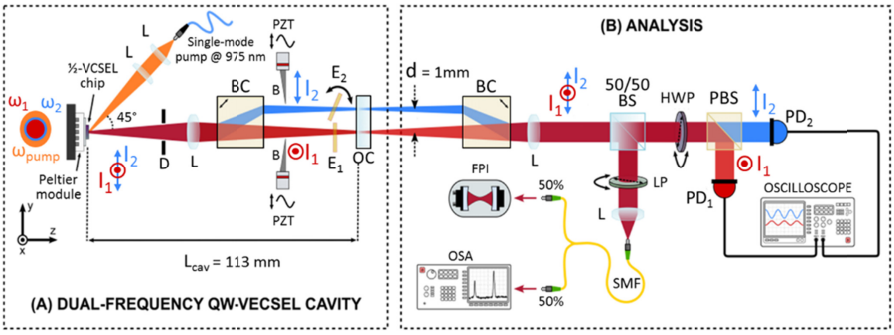

Fig. 1. Experimental setup used to perform the coupling constant measurements in the 1.54 µm-emitting dual-frequency QW-VECSEL. L: lens, D: diaphragm, BC: YVO_4 birefringent crystal, PZT: piezo-actuator, B: razor blade, E: etalon, OC: planar output coupler, BS: beam splitter, LP: linear polarizer, FPI: Fabry-Perot interferometer, OSA: optical spectrum analyzer, HWP: half-wave plate, PBS: polarizing beam splitter, PD: balanced InGaAs photodiode. d accounts for the spatial separation between the two modes. Index 1 and 2 are referred to the two orthogonally-polarized eigenmodes, respectively ordinary and extraordinary. I_1 and I_2 are the intensity of mode 1 and 2 respectively.

The analysis part of the experimental setup is depicted in Fig. 1. It includes a second YVO_4 birefringent crystal, similar to the first one, used to spatially recombine the two eigenmodes. After a collimating lens and a 50/50 beam splitter, part of the signal is coupled into a single-mode fiber and sent to a spectral analysis line composed of an optical spectrum analyzer (OSA) and a 7 GHz free spectral range scanning Fabry-Perot interferometer (FPI). The FPI enables monitoring the proper single frequency operation of each mode of the VECSEL and in particular to check that no mode-hopping occur during measurements. A linear polarizer, placed before the injection lens, allows discriminating between the two eigenmodes. The remaining part of the signal is sent to a polarizing beam splitter (PBS), which separates the two eigenmodes towards two balanced InGaAs photodiodes (PD_1 and PD_2, respectively) connected to a digital oscilloscope. A half-wave plate is inserted in front of the PBS for calibration purpose. By rotating this waveplate, the two polarizations are commutated in the two detection arms. Any residual gain/efficiency unbalance between the two arms is then measured and taken into account in the measurements.

Without etalons the laser naturally operates in the longitudinally multimode regime, characterized by a wide emission spectrum centered at 1540 nm (see Fig. 2(b)). In this condition, the laser exhibits a threshold at around 200 mW. Due to the numerous components inside the cavity, the total emitted power reaches only 14.7 mW for 1050 mW of incident pump power (black curve of Fig. 2(a)). The semiconductor structure being not coated for the pump wavelength, approximately half of the pump power is transmitted into the active medium. The insertion of the two etalons on both arms of the cavity forces the VECSEL to oscillate in the dual-frequency regime (see Fig. 2(c)). The maximum achievable output power

Optics EXPRESS

becomes 3.6 mW (red curve in Fig. 2(a)), whereas the threshold is slightly increased to 220 mW of incident power. Single-frequency operation of each mode is confirmed by the FPI spectrum shown in Fig. 2(e), indicating the simultaneous lasing of the ordinary and extraordinary eigenmodes, which in illustration are separated by $\Delta\lambda$ = 8.38 nm around the central emission wavelength (see Fig. 2(d)).

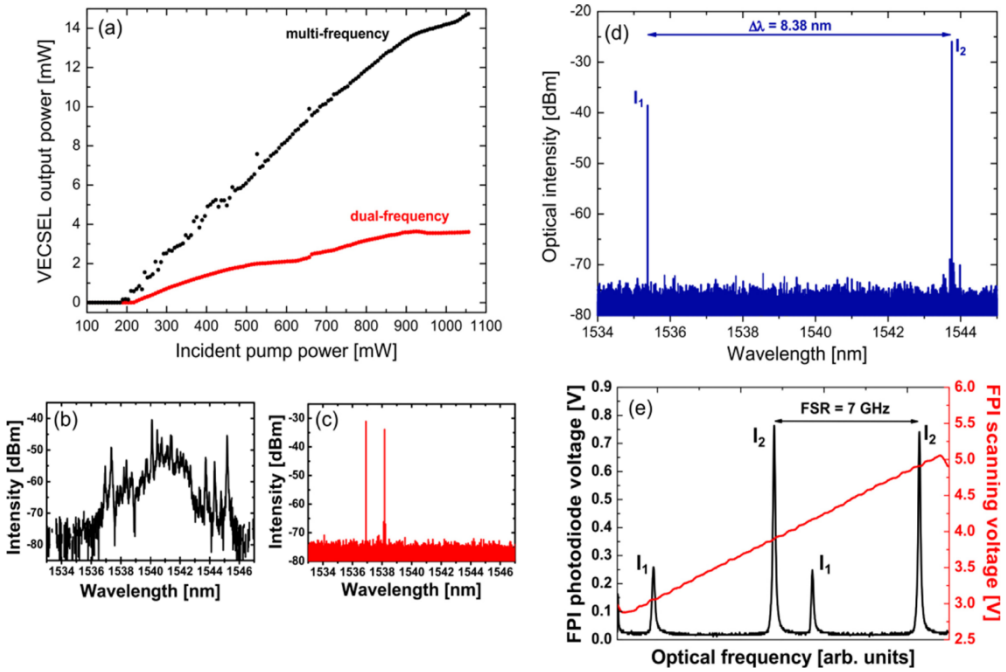

Fig. 2. (a) Typical output characteristics of the QW-VECSEL as a function of the incident pump power when operating in multi-frequency (black curve) and dual-frequency modes (red curve). (b) and (c) corresponding OSA spectra for multi-frequency and dual-frequency operation. (d) Dual-frequency spectrum of the two eigenmodes, acquired by the OSA in the case of a wavelength difference $\Delta\lambda$ = 8.38 nm. (e) Fabry-Perot spectrum showing single frequency oscillation of each polarization.

It is worth mentioning that the simultaneous oscillation of the two modes is achieved with a careful balance of optical losses on both arms. To this aim the central position of the razor blades is adjusted in order to introduce sufficient optical losses on the dominant eigenmode, the residual gain dissymmetry being mainly determined by the natural strain as well as the pump induced strain in the QW chip. Thermal fluctuations and mechanical vibrations might disrupt such a balance, resulting in the loss of the dual-frequency operation. Our experiment being not shielded the simultaneous oscillation of the two modes lasts from a few minutes to a few tens of minutes which make it possible to accurately perform the coupling constant measurement. This first observation is also a preliminary indication that the coupling between the two eigenstates is relatively strong (C close to 1), as expected in QWs-based active media. This point is further discussed in the following section.

3. Measurement of the coupling constant and results

The rate equations governing the evolution of the intensities I_1 and I_2 of the two eigenmodes in a class-A dual-frequency laser can be written as [27]:

$$\frac{\partial I_1}{\partial t} = I_1\left[\alpha_1 - \beta_1 I_1 - \theta_{12} I_2\right] \tag{1a}$$

Optics EXPRESS

$$\frac{\partial I_2}{\partial t} = I_2\left[\alpha_2 - \beta_2 I_2 - \theta_{21} I_1\right] \tag{1b}$$

where α_1 and α_2 are the unsaturated gains minus losses for each mode. β and θ are respectively the self- and cross-saturation coefficients. The steady-state solution of the two coupled Eqs. (1a, b) corresponding to the simultaneous oscillation of the two modes reads:

$$I_1 = \frac{\alpha_1/\beta_1 - K_{12}\alpha_2/\beta_2}{1-C} \tag{2a}$$

$$I_2 = \frac{\alpha_2/\beta_2 - K_{21}\alpha_1/\beta_1}{1-C} \tag{2b}$$

where K_{12} and K_{21} are the cross- to self- saturation ratios and C is the Lamb coupling constant defined as [11]:

$$C = K_{12}K_{21} \tag{3}$$

By introducing extra optical losses on the extraordinary mode we deduce, from Eqs. (2a) and (2b), the expression of K_{12} with respect to the variation of I_1 and I_2:

$$K_{12} = -\frac{\partial I_1 / \partial \alpha_2}{\partial I_2 / \partial \alpha_2} \tag{4a}$$

Conversely, K_{21} is obtained by modulating the losses on the ordinary mode:

$$K_{21} = -\frac{\partial I_2 / \partial \alpha_1}{\partial I_1 / \partial \alpha_1} \tag{4b}$$

The spatial separation, introduced by the YVO_4 crystal, enables us to modulate the optical losses of one arm at a time by modulating the position of the razor blade. During the whole experiment, the intensity modulation index is kept below 10%, in order to avoid any modification of the spatial profile of the beams. The losses are modulated at 19 Hz, thus being slow enough compared to the time constants of the laser and allowing us to consider the steady-state solutions (2a, b) presented before. The incident pump power is set to 900 mW, corresponding to more than four times the threshold pump power, namely a pumping rate r = 4.1. The CW output power of each mode ranges from 40 µW to 600 µW depending on the mode's wavelength and the losses introduced to get balanced dual-frequency operation. Figures 3(a) and 3(b) show typical experimental traces of I_1 and I_2 which are in opposite phase as expected from the Eqs. (4a) and (4b). The Lissajous curves of the modulated signals where the x-axis accounts for the modulated signal related to loss modulation in the corresponding cavity arm, are segments whose slopes give the cross- to self-saturation ratios K_{12} and K_{21} (see Fig. 3(c)). The coupling constant C is then calculated from the product of the two slopes. In this illustration, a coupling constant of 0.83 is measured for a wavelength difference $\Delta\lambda$ between the two modes of 2 nm. It is worthwhile mentioning that the slopes K_{12} and K_{21} remain constant within the achievable power excursion of I_1 and I_2. Consequently, neither the cross-to-self saturation terms nor C depend on the laser operation point, within the limit of our achievable pumping rate.

Optics EXPRESS

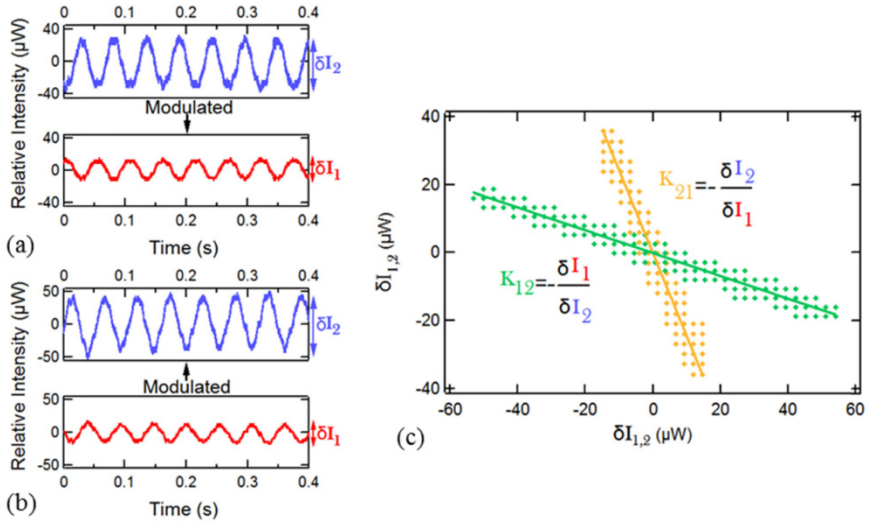

Fig. 3. Evolution of I_1 and I_2 observed at the oscilloscope when the modulation losses are applied to (a) mode *1* or (b) mode *2* for a wavelength difference of 2 nm. (c) Relative unmodulated mode intensity versus the relative modulated mode intensity ($\delta I_{1,2}$); the value of each slope leads to the respective cross- to self- saturation ratios.

We have achieved the dual-frequency operation for $\Delta\lambda$ ranging from 0.36 nm to 10.8 nm. Above 10.8 nm, the edges of the gain spectrum are almost reached (see multi-frequency emission on Fig. 2b) forbidding dual-frequency operation. Some of the spectra acquired with the OSA are shown in Fig. 4(a). The black colored spectrum is related to the ordinary mode 1 whose wavelength is fixed to 1535.4 ± 0.2 nm. The blue colored spectrum is related to the extraordinary mode 2 whose wavelength is adjusted from 1535.6 nm to 1546.3 nm by rotating the etalon located on the extraordinary mode. For these $\Delta\lambda$, we measured the two cross- to self-saturation ratios. We witnessed that they evolve in opposite ways, depending on the wavelength difference. Moreover, K_{21} is always superior to K_{12}, as shown in Fig. 4(b) and their values are rather different: $1.93 < K_{21} < 2.81$ and $0.29 < K_{12} < 0.44$. K_{21} is at least 4.3 times higher than its corresponding K_{12}.

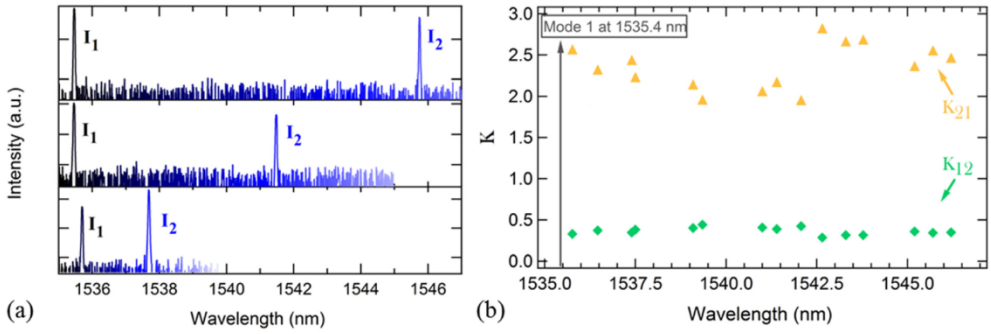

Fig. 4. (a) Emission spectra illustrated for three wavelength differences: 2, 6 and 9.8 nm from bottom to up. (b) Evolution of the two cross- to self-saturations ratios versus the wavelength of mode 2. The wavelength of mode 1 is set at 1535.4 ± 0.2 nm.

Moreover, the same behavior is observed when the wavelengths of mode 1 and 2 are swapped, proving that the observed dissymmetry is not ruled by the mode of highest energy level. Further studies are required to understand the origin of this significant dissymmetry between K_{12} and K_{21}. The theoretical developments [28] and [29] could bring some insights

Optics EXPRESS

on the different values of K_{12} and K_{21} although they currently fail to predict such a large dissymmetry considering our experimental conditions.

From these cross- to self-saturation ratios we calculate the coupling constant with respect to $\Delta\lambda$. The results are presented in Fig. 5(a). It turns out that for wavelength differences ranging from 0.36 nm to 10.8 nm, the Lamb coupling constant remains constant with a very narrow dispersion even though K_{12} and K_{21} are wavelength dependent, leading to a mean value of 0.839. This constant is very close to that reported value in Ref [22], despite the different nature of active medium material (GaAs-based versus InP-based in this study). At first glance, we can notice that this constant could be related mainly to the design of the active gain medium (QW) rather than to the nature of the material itself. The stability of such dual-wavelength laser might be increased by reducing Lamb's constant using a different nature of gain medium. For instance, semiconductor based quantum dots (QDs) have been shown to present significant differences as compared QW. In particular their homogeneous and inhomogeneous broadening lead to unusual behaviors in lasers characteristics [30] as well as in optical amplifiers [31]. QDs active layers might be very promising for dual frequency lasers in terms of oscillation robustness in agreement with the theoretical predictions of Ref [29].

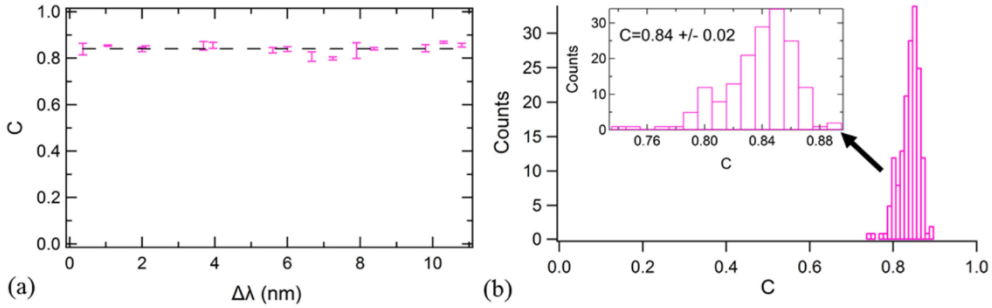

Fig. 5. (a) Lamb coupling constant C versus wavelength difference between the two modes. Error bars represent the standard deviation of all the values measured for one wavelength difference. The dashed line stands for C = 0.84. (b) Histogram of the C values with equal intervals of 0.01.

Going further, we acquired a statistically representative number of measurements to ensure the accuracy of the value of the coupling constant and to avoid the impact of random environmental disturbances on the final value. In that respect, we acquired a total of 168 values with approximately 10 values per $\Delta\lambda$. The related standard deviation is given by the error bars in Fig. 5(a) highlighting the accuracy of each measurement. Figure 5(b) represents the dispersion of C values regardless the wavelength's difference between the modes, sorted in equal intervals of 0.01. The overall standard deviation of 0.02 is relatively small, showing that the Lamb coupling constant does not depend on $\Delta\lambda$ and that $C = 0.84 \pm 0.02$.

4. Conclusion

In conclusion, we report for the first time to our knowledge the direct measurement of the Lamb coupling constant C for an OP-QW-based VECSEL emitting around 1.54 µm. We carefully designed the laser cavity to ensure the simultaneous emission of two modes sharing the same active region while sufficiently separated in the rest of the cavity to independently tune their wavelengths. It allowed us to measure the spectral dependence of the coupling constant through the cross- to self-saturation ratios K_{12} and K_{21} for a wavelength difference $\Delta\lambda$ ranging from 0.36 nm and up to 10.8 nm. We found that K_{21} is always at least 4.3 times higher than its corresponding K_{12}, and they both change depending on $\Delta\lambda$. Despite this, their product C remains constant and is $C = 0.84 \pm 0.02$. In perspective, the origin of the significant difference between the two cross- to self-saturation ratios must be understood with further

Optics EXPRESS

experiments. Moreover, as QD active media are expected to ease dual wavelength operation, we also consider performing the same mode coupling experiments with QD active media which exhibit wider gains and different homogeneous broadening features as compared to QW [32]. Indeed, the Lamb coupling constant in QDs might be weaker than in QWs for large spectral separations. Accordingly, the implementation of such active media could be of great interest for engineering robust dual-frequency class-A VECSEL.

Funding

Agence Nationale de la Recherche (ANR) and Swiss National Science Foundation (SNSF) (ANR-SNSF IDYLIC project, grant ANR-15-CE24-0034-01).

References

1. W. E. Lamb, "Theory of an Optical Maser," Phys. Rev. **134**(6A), A1429–A1450 (1964).
2. M. Alouini, M. Brunel, F. Bretenaker, M. Vallet, and A. L. Floch, "Dual tunable wavelength Er,Yb:glass laser for terahertz beat frequency generation," IEEE Photonics Technol. Lett. **10**(11), 1554–1556 (1998).
3. P. H. Siegel, "Terahertz technology," IEEE Trans. Microw. Theory Tech. **50**(3), 910–928 (2002).
4. J. W. Waters, L. Froidevaux, R. S. Harwood, R. F. Jarnot, H. M. Pickett, W. G. Read, P. H. Siegel, R. E. Cofield, M. J. Filipiak, D. A. Flower, J. R. Holden, G. K. Lau, N. J. Livesey, G. L. Manney, H. C. Pumphrey, M. L. Santee, D. L. Wu, D. T. Cuddy, R. R. Lay, M. S. Loo, V. S. Perun, M. J. Schwartz, P. C. Stek, R. P. Thurstans, M. A. Boyles, K. M. Chandra, M. C. Chavez, Gun-Shing Chen, B. V. Chudasama, R. Dodge, R. A. Fuller, M. A. Girard, J. H. Jiang, Yibo Jiang, B. W. Knosp, R. C. LaBelle, J. C. Lam, K. A. Lee, D. Miller, J. E. Oswald, N. C. Patel, D. M. Pukala, O. Quintero, D. M. Scaff, W. Van Snyder, M. C. Tope, P. A. Wagner, and M. J. Walch, "The Earth observing system microwave limb sounder (EOS MLS) on the aura Satellite," IEEE Trans. Geosci. Remote Sens. **44**(5), 1075–1092 (2006).
5. H. J. Song and T. Nagatsuma, "Present and Future of Terahertz Communications," IEEE Trans. Terahertz Sci. Technol. **1**(1), 256–263 (2011).
6. J.-H. Son, "Terahertz electromagnetic interactions with biological matter and their applications," J. Appl. Phys. **105**(10), 102033 (2009).
7. J. F. Federici, B. Schulkin, F. Huang, D. Gary, R. Barat, F. Oliveira, and D. Zimdars, "THz imaging and sensing for security applications—explosives, weapons and drugs," Semicond. Sci. Technol. **20**(7), S266–S280 (2005).
8. M. Brunel, F. Bretenaker, and A. Le Floch, "Tunable optical microwave source using spatially resolved laser eigenstates," Opt. Lett. **22**(6), 384–386 (1997).
9. M. Alouini, F. Bretenaker, M. Brunel, A. Le Floch, M. Vallet, and P. Thony, "Existence of two coupling constants in microchip lasers," Opt. Lett. **25**(12), 896–898 (2000).
10. K.-G. Hong, S.-T. Lin, and M.-D. Wei, "Polarization bistability associated with $^4F_{3/2}\rightarrow{}^4I_{11/2}$ and $^4F_{3/2}\rightarrow{}^4I_{13/2}$ transitions in Nd:YVO_4 laser with intra-cavity periodically poled lithium niobate Bragg modulator," Opt. Express **23**(14), 17979–17987 (2015).
11. M. Sargent, M. O. Scully, and W. E. Lamb, *Laser Physics* (London : Addison-Wesley, 1974).
12. M. Alouini, PhD thesis *Theoretical and Experimental Study of Er $^{3+}$ and Nd $^{3+}$ Solid-State Lasers: Application of Dual-Frequency Lasers to Optical and Microwave Telecommunications* (University of Rennes 1, 2001).
13. M. Brunel, A. Amon, and M. Vallet, "Dual-polarization microchip laser at 1.53 μm," Opt. Lett. **30**(18), 2418–2420 (2005).
14. A. McKay, J. M. Dawes, and J.-D. Park, "Polarisation-mode coupling in (100)-cut Nd:YAG," Opt. Express **15**(25), 16342–16347 (2007).
15. G. Baili, L. Morvan, M. Alouini, D. Dolfi, F. Bretenaker, I. Sagnes, and A. Garnache, "Experimental demonstration of a tunable dual-frequency semiconductor laser free of relaxation oscillations," Opt. Lett. **34**(21), 3421–3423 (2009).
16. S. De, V. Pal, A. El Amili, G. Pillet, G. Baili, M. Alouini, I. Sagnes, R. Ghosh, and F. Bretenaker, "Intensity noise correlations in a two-frequency VECSEL," Opt. Express **21**(3), 2538–2550 (2013).
17. S. De, A. E. Amili, I. Fsaifes, G. Pillet, G. Baili, F. Goldfarb, M. Alouini, I. Sagnes, and F. Bretenaker, "Phase Noise of the Radio Frequency (RF) Beatnote Generated by a Dual-Frequency VECSEL," J. Lit. Technol. **32**(7), 1307–1316 (2014).
18. F. A. Camargo, J. Barrientos, G. Baili, L. Morvan, D. Dolfi, D. Holleville, S. Guerandel, I. Sagnes, P. Georges, and G. Lucas-Leclin, "Coherent Dual-Frequency Emission of a Vertical External-Cavity Semiconductor Laser at the Cesium D_2 Line," IEEE Photonics Technol. Lett. **24**(14), 1218–1220 (2012).
19. P. Dumont, F. Camargo, J.-M. Danet, D. Holleville, S. Guerandel, G. Pillet, G. Baili, L. Morvan, D. Dolfi, I. Gozhyk, G. Beaudoin, I. Sagnes, P. Georges, and G. Lucas-Leclin, "Low-Noise Dual-Frequency Laser for Compact Cs Atomic Clocks," J. Lit. Technol. **32**(20), 3817–3823 (2014).
20. S. De, G. Baili, M. Alouini, J.-C. Harmand, S. Bouchoule, and F. Bretenaker, "Class-A dual-frequency VECSEL at telecom wavelength," Opt. Lett. **39**(19), 5586–5589 (2014).

Optics EXPRESS

21. H. Liu, G. Gredat, S. De, I. Fsaifes, A. Ly, R. Vatré, G. Baili, S. Bouchoule, F. Goldfarb, and F. Bretenaker, "Ultra-low noise dual-frequency VECSEL at telecom wavelength using fully correlated pumping," Opt. Lett. **43**(8), 1794–1797 (2018).
22. V. Pal, P. Trofimoff, B.-X. Miranda, G. Baili, M. Alouini, L. Morvan, D. Dolfi, F. Goldfarb, I. Sagnes, R. Ghosh, and F. Bretenaker, "Measurement of the coupling constant in a two-frequency VECSEL," Opt. Express **18**(5), 5008–5014 (2010).
23. A. Sirbu, A. Rantamäki, E. J. Saarinen, V. Iakovlev, A. Mereuta, J. Lyytikäinen, A. Caliman, N. Volet, O. G. Okhotnikov, and E. Kapon, "High performance wafer-fused semiconductor disk lasers emitting in the 1300 nm waveband," Opt. Express **22**(24), 29398–29403 (2014).
24. S. T. Keller, A. Sirbu, V. Iakovlev, A. Caliman, A. Mereuta, and E. Kapon, "8.5 W VECSEL output at 1270 nm with conversion efficiency of 59%," Opt. Express **23**(13), 17437–17442 (2015).
25. H. Kogelnik and T. Li, "Laser Beams and Resonators," Appl. Opt. **5**(10), 1550–1567 (1966).
26. C. Hessenius, N. Terry, M. Fallahi, J. Moloney, and R. Bedford, "Gain coupling of class A semiconductor lasers," Opt. Lett. **35**(18), 3060–3062 (2010).
27. A. E. Siegman, *Lasers* (University Science Books, 1986).
28. S. De, V. Potapchuk, and F. Bretenaker, "Influence of spin-dependent carrier dynamics on the properties of a dual-frequency vertical-external-cavity surface-emitting laser," Phys. Rev. A **90**(1), 013841 (2014).
29. L. Chusseau, A. Vallet, M. Perrin, C. Paranthoën, and M. Alouini, "Lamb mode-coupling constant in quantum-dot semiconductor lasers," Phys. Rev. B **98**(15), 155306 (2018).
30. A. Matsumoto, K. Akahane, T. Umezawa, and N. Yamamoto, "Extremely stable temperature characteristics of 1550-nm band, p-doped, highly stacked quantum-dot laser diodes," Jpn. J. Appl. Phys. **56**(4S), 04CH07 (2017).
31. G. Contestabile, A. Maruta, S. Sekiguchi, K. Morito, M. Sugawara, and K. Kitayama, "Cross-Gain Modulation in Quantum-Dot SOA at 1550 nm," IEEE J. Quantum Electron. **46**(12), 1696–1703 (2010).
32. M. Sugawara, K. Mukai, Y. Nakata, H. Ishikawa, and A. Sakamoto, "Effect of homogeneous broadening of optical gain on lasing spectra in self-assembled InGaAs/GaAs quantum dot lasers," Phys. Rev. B Condens. Matter Mater. Phys. **61**(11), 7595–7603 (2000).